ARTICLE OPEN

Check for updates

Electronic and magnetic properties of the RuX_3 (X = Cl, Br, I) family: two siblings—and a cousin?

David A. S. Kaib[1]✉, Kira Riedl[1]✉, Aleksandar Razpopov[1], Ying Li[2], Steffen Backes[3], Igor I. Mazin[4] and Roser Valentí[1]✉

Motivated by reports of metallic behavior in the recently synthesized RuI_3, in contrast to the Mott-insulating nature of the actively discussed α-$RuCl_3$, as well as $RuBr_3$, we present a detailed comparative analysis of the electronic and magnetic properties of this family of trihalides. Using a combination of first-principles calculations and effective-model considerations, we conclude that RuI_3, similarly to the other two members, is most probably on the verge of a Mott insulator, but with much smaller magnetic moments and strong magnetic frustration. We predict the ideal pristine crystal of RuI_3 to have a nearly vanishing conventional nearest-neighbor Heisenberg interaction and to be a quantum spin liquid candidate of a possibly different kind than the Kitaev spin liquid. In order to understand the apparent contradiction to the reported resistivity ρ, we analyze the experimental evidence for all three compounds and propose a scenario for the observed metallicity in existing samples of RuI_3. Furthermore, for the Mott insulator $RuBr_3$, we obtain a magnetic Hamiltonian of a similar form to that in the much-discussed α-$RuCl_3$ and show that this Hamiltonian is in agreement with experimental evidence in $RuBr_3$.

npj Quantum Materials (2022)7:75 ; https://doi.org/10.1038/s41535-022-00481-3

INTRODUCTION

RuI_3 and $RuBr_3$ are recent additions to the RuX_3 family (X = Cl, Br, I) of layered Ru-based trihalides (Fig. 1a). The first member, α-$RuCl_3$ (in the following '$RuCl_3$') has attracted considerable attention in recent years as a candidate material for the Kitaev honeycomb model[1]. $RuCl_3$ is a spin–orbit-assisted Mott insulator[2–5] whose magnetic low-energy degrees of freedom can be described in terms of $j_{\mathrm{eff}} = 1/2$ moments that interact through strongly anisotropic exchange[2,6–8]. While the material enters a so-called zigzag antiferromagnetic order (Fig. 1b) at low temperatures $T_N \approx 7$ K[4,9,10], various experiments at finite temperature[11–14] or at finite magnetic field[4,15–18] have been interpreted as hallmarks of Kitaev physics, a subject which is presently under intensive debate[19–24].

Recently, a sister compound with a heavier halogen, X = Br, was synthesized[25]. Analogous to $RuCl_3$, it is insulating and shows zigzag magnetic order, albeit with higher Néel temperature $T_N = 34$ K[25]. In contrast to $RuCl_3$, the authors of ref. [25] reported a Weiss constant with dominant antiferromagnetic interactions and a direction of the zigzag-ordered moment different from $RuCl_3$ and argued that this deviation suggests closer proximity to the pure Kitaev model.

To complete the RuX_3 family, two independent groups have now synthesized RuI_3 with the even heavier halogen iodine[26,27]. In contrast to the two 'sibling' compounds, a quasi-metallic behavior was observed in RuI_3, questioning the description in terms of localized $j_{\mathrm{eff}} = 1/2$ moments. Even though the dc resistivities measured in RuI_3 are orders of magnitude smaller than those of $RuCl_3$ or $RuBr_3$, the reported values of 10^{-3}–$10^{-2}\,\Omega\,\mathrm{cm}$[26] are uncharacteristically large for metals or even typical bad metals[28], and practically temperature-independent. While neither of the groups found clear signatures of magnetic ordering[26,27], they reported different behaviors of the magnetic susceptibility, which is either found to be temperature-independent[26] or with a strong upturn at low temperatures[27], suggesting that sample quality plays a crucial role.

In order to understand the apparently distinct behavior of this family of trihalide materials, in this work, we analyze the available experimental data and perform a detailed comparative study of the electronic and magnetic properties of the systems via first-principles calculations and extracted low-energy models. We find that: (i) The behavior of RuI_3 is not that far from $RuCl_3$ and $RuBr_3$ and the variations across the series are more quantitative than qualitative. (ii) Pristine samples of RuI_3 should be insulating with highly anisotropic magnetic exchange and nearly vanishing conventional Heisenberg interaction. We argue that the reported metallic behavior in RuI_3 could have its origin in sample quality. (iii) The magnetism in the Mott insulator $RuBr_3$ has predominantly ferromagnetic interactions, in contrast to what is suggested by the Curie–Weiss analysis of ref. [25]. We show that such interactions are consistent with experiment when taking into account spin-orbit coupling effects in the Curie–Weiss behavior.

Our study derives model parameters and magnetic Hamiltonians for the whole RuX_3 family from ab-initio, which will be useful for future theoretical studies of these systems. In contrast to the usual model derivations that only include local spin–orbit coupling (SOC) on the magnetic ion[2,6,8], our approach includes all SOC effects in the crystal. In fact, we show that SOC from the ligands leads to significant deviations from the Ruthenium-only SOC picture in the case of $RuBr_3$ and RuI_3.

RESULTS AND DISCUSSION

Comparative analysis of experiments

In the following, we analyze the reported electrical resistivity, specific heat, and magnetic susceptibility data for RuX_3 (X = Cl, Br, I)[10,25–27,29].

[1]Institut für Theoretische Physik, Goethe-Universität Frankfurt, 60438 Frankfurt am Main, Germany. [2]Department of Applied Physics and MOE Key Laboratory for Nonequilibrium Synthesis and Modulation of Condensed Matter, School of Physics, Xi'an Jiaotong University, 710049 Xi'an, China. [3]CPHT, CNRS, Ecole Polytechnique, Institut Polytechnique de Paris, Route de Saclay, 91128 Palaiseau, France. [4]Department of Physics and Astronomy and Quantum Science and Engineering Center, George Mason University, Fairfax, Virginia 22030, USA. ✉email: kaib@itp.uni-frankfurt.de; riedl@itp.uni-frankfurt.de; valenti@itp.uni-frankfurt.de

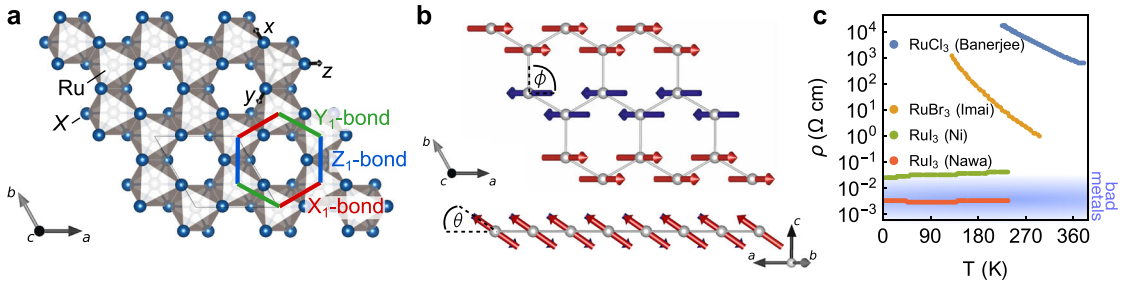

Fig. 1 RuX_3 (X = Cl, Br, I) crystal structure, magnetic structure, and resistivity. a Honeycomb layer in the RuX_3 (X = Cl, Br, I) trihalides with bond definitions, cubic axes (*xyz*) and crystallographic axes (*abc*) in the $R\bar{3}$ structure, **b** Zigzag magnetic order in a honeycomb layer from two perspectives, with definitions of in-plane-angle ϕ and out-of-plane-angle θ. **c** Comparison of experimental dc resistivities as a function of temperature. Data was extracted from plots in the following references and labeled by respective first-author names: $RuCl_3$[10], $RuBr_3$[25], and RuI_3[26,27]. The shaded background depicts a typical range of resistivity for bad metals[28].

In Fig. 1c we summarize the temperature dependence of the experimental resistivity data[10,25–27] in all three compounds. In RuI_3, the resistivity has a weak[27] or almost no[26] temperature dependence (Fig. 1c). Traditionally, metals are classified as materials where the resistivity ρ increases with temperature, distinguishing conventional metals (e.g., Cu) as those where in clean samples at temperatures roughly 300–600 K, $\rho \sim 10^{-6}$ to $\sim 10^{-5}\,\Omega$ cm, and bad metals as those with resistivities of $\sim 1-10\,\text{m}\Omega$ cm. This range is shown as a background shading in Fig. 1c. The reported resistivities for RuI_3 ($\rho \sim 40\,\text{m}\Omega\,\text{cm}$[27] and $\rho \sim 4\,\text{m}\Omega\,\text{cm}$[26]) are high even for bad metals, surpassing the Ioffe–Regel limit by more than an order of magnitude. Even more relevant, the lower-resistivity set of data[26] shows no discernible temperature dependence at all, while the data in ref. [27] show a very weak positive derivative $d\rho/dT$, but the absolute value is above anything traditionally considered metallic.

Seemingly, as also pointed out in ref. [27], electron transport in existing RuI_3 samples may be contaminated by grain boundaries. One possibility to interpret the measurements is that the pristine material is metallic, but insulating grain boundaries prevent percolation. Then, the in-grain resistivity can be neglected and what is measured is the resistivity of the insulating grain boundaries. In that case, however, thermal activation of carriers in the boundaries should give a positive temperature gradient of the resistivity, which is not observed. The opposite scenario is that of an insulating behavior in the bulk and (possibly bad) metallic one between the grains. In that case, the large resistivity reflects the small relative volume of metallic boundaries, where the transport is dominated by the residual resistivity. This scenario is compatible with the observations. Morphology of the grain boundaries can vary wildly depending on the growth conditions, including but not limited to vacancies, twins, dislocation, and plain chemical dirt. Grain boundaries in semiconductors are often observed to be metallic. Apart from grain boundaries contaminating resistivity measurements, disorder (in form of vacancies, stacking faults, etc.[26,27]) could promote the bulk metallic phase over the Mott-insulating one, as has been shown for example for the Mott insulator κ-(BEDT-TTF)$_2$Cu[N(CN)$_2$]Cl[30]. Indeed, in our first-principles calculations discussed below, we find the ideal RuI_3 to already be quite close to a Mott–metal transition.

Turning to the sibling compounds $RuCl_3$ and $RuBr_3$, the resistivity (Fig. 1c) decreases with temperature, as expected for Mott insulators, and both systems show an approximate exponential activation gap behavior, $E_{g,\text{eff}}(T) = -k_B T^2 (d \ln \rho / dT)$, although with a significant blue-shift of the gap with increasing temperatures.

Considering specific heat data in the compounds, the specific heat for $RuCl_3$ displays a well-defined peak at $T_N \approx 7$ K denoting the onset of the zigzag order, while the onset of long-range magnetic order in $RuBr_3$ is observed by a kink at $T_N = 34$ K[25]. None of this is observed for RuI_3[26,27]. In Table 1 we summarize specific heat parameters reported experimentally[25–27,31], where γ (β) is the T-linear (T^3) contribution to $C(T)$.

Table 1. Overview of reported specific heat parameters.

Sample	γ	β	T_D	$T_D M_{RuX_3}^{1/2}$
$RuCl_3$[a] [31]		1.22	185	1
$RuBr_3$ [25]		1.93	159	1.21
RuI_3 [27]	29.3	4.72	118	1.07
RuI_3 [26]	17.7	3.66	129	1.17

γ (β) is the coefficient of the T-linear (T^3) contribution and given in units of $\text{mJ K}^{-2}\text{mol}^{-1}$ ($\text{mJ K}^{-4}\,\text{mol}^{-1}$). Debye temperature $T_D = \left(\frac{12\pi^4 NR}{5\beta}\right)^{1/3}$ is given in Kelvin and $T_D M_{RuX_3}^{1/2}$ as a ratio to the value for $RuCl_3$ (first row), where M_{RuX_3} is the harmonic average of the RuX_3 mass.
[a]Note that the values given for $RuCl_3$ correspond to the asymptotic field-polarized limit extracted by Tanaka et al.[31], as otherwise at zero field the low-temperature specific heat behavior is dominated by vicinity to the Néel temperature of $RuCl_3$, causing large magnetic contributions to β.

In RuI_3, the T-linear contribution, even though contaminated by an extrinsic raise at small temperatures in ref. [27] attributed to the nuclear quadrupole moment of Ru, yields $\gamma \sim 15-30\,\text{mJ K}^{-2}\,\text{mol}^{-1}$ [26,27]. From our electronic structure calculations of RuI_3 shown below, we find that the unrenormalized metallic (i.e., nonmagnetic, not U-corrected) density of states corresponds to $\gamma_0 \approx 3\,\text{mJ K}^{-3}\,\text{mol}^{-1}$, suggesting a mass renormalization (if this γ is intrinsic) of a factor of 7–12. In the scenario where the metallic grain boundaries take up a sizeable fraction of the sample volume, this renormalization shall be even stronger, encroaching into the heavy fermions domain. This suggests that the origin of the anomalously large residual heat capacity may not be related to intrinsic metallicity. It is worth noting that the T^3 term β of $C(T)$, on the other hand, is rather reasonable for the three systems and scales roughly as the harmonic average M_{RuX_3} of the atomic masses (last column in Table 1).

We now turn our attention to magnetic susceptibility measurements. Figure 2a summarizes the powder-averaged measured magnetic susceptibilities $\chi(T)$ as reported in refs. [25–27,32]. At low temperatures, the $RuCl_3$ data[32] shows a clear signature of a transition to the ordered magnetic phase at 7 K. For $RuBr_3$, the Néel transition $T_N \approx 34$ K is less apparent from the susceptibility, but the maximum in $d\chi/dT$ is consistent with the distinct transition seen in NMR relaxation measurements[25]. The experimental report on powder samples of $RuBr_3$ utilized a standard Curie–Weiss (CW) fit, yielding an average Curie–Weiss temperature $\Theta_{\text{std}}^{\text{avg}} = -58$ K[25], indicating predominantly AFM interactions. However, as we have recently shown[33], the Weiss constants obtained with such a standard CW fit may not anymore reflect the intrinsic exchange couplings in the case of significant SOC in the material, as is the

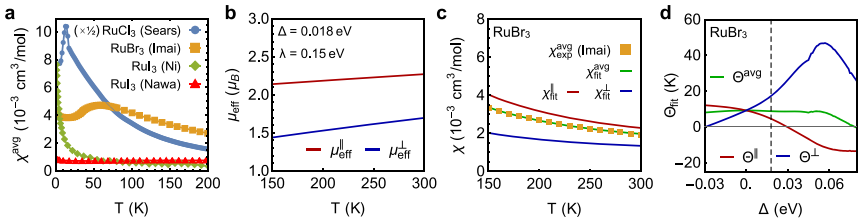

Fig. 2 Magnetic susceptibility and modified Curie–Weiss fit. a Experimental direction-averaged RuX_3 susceptibility data, extracted from plots in the following references and labeled by respective first-author names: $RuCl_3$[32], $RuBr_3$[25], RuI_3[27], RuI_3[26]. Note that the $RuCl_3$ curve is scaled by $\frac{1}{2}$. **b** Calculated temperature-dependent effective moment $\mu_{\mathrm{eff}}(T)$ for $\Delta = 0.018$ eV and SOC $\lambda = 0.15$ eV. **c** Modified Curie–Weiss fit of $RuBr_3$ data, taking into account such $\mu_{\mathrm{eff}}(T)$. **d** Dependence of best-fit Weiss constants on assumed Δ. The vertical dashed line indicates $\Delta = 0.018$ eV.

case for the Ru-based trihalides. With SOC, temperature-dependent van-Vleck contributions can arise, which can be effectively captured in a temperature-dependent magnetic moment $\mu_{\mathrm{eff}}(T, \Delta)$[33], as shown for $\Delta = 0.018$ eV in Fig. 2b, where Δ can be directly associated to the crystal field splitting resulting from the distorted octahedral environment of Ru. In fact, for the sister compound $RuCl_3$, a standard CW fit would lead to $\Theta^{\mathrm{avg}}_{\mathrm{std}} = -20$ K, whereas an improved CW fit taking into account such van-Vleck-like contributions[33] provides CW constants $\Theta^{\parallel} = +55$ K for the magnetic field in the honeycomb plane and $\Theta^{\perp} = +33$ K for the out-of-plane field, revealing an average CW constant, $\Theta^{\mathrm{avg}} = \frac{2\Theta^{\parallel}+\Theta^{\perp}}{3}$, of ≈48K. This indicates predominant ferromagnetic (FM) interactions, as they have become established for the magnetic Hamiltonian in $RuCl_3$[34–37].

Considering a similar strategy (see the "Methods" section), we fit the average susceptibility χ^{avg} of $RuBr_3$[25]. However, since the crystal-field parameter Δ primarily controls the in-plane vs. out-of-plane anisotropy, and for $RuBr_3$ only powder-averaged data are available, we do not aim at extracting Δ by fitting. Instead, we first fix Δ using our first-principles calculations, enforcing $\mu^{\parallel}_{\mathrm{eff}}/\mu^{\perp}_{\mathrm{eff}}(T = 0\,\mathrm{K}) \propto g_{\parallel}/g_{\perp}$, where $g_{\parallel}/g_{\perp}$ are taken from quantum chemistry calculations (see Fig. 5a, discussed below). This leads to $\Delta = 0.018$ eV. The best CW fit accounting for the implied $\mu_{\mathrm{eff}}(T, \Delta = 0.018\,\mathrm{eV})$ (shown in Fig. 2c) yields Weiss constants $\Theta^{\parallel} \approx 5$ K, $\Theta^{\perp} \approx 17$ K and $\Theta^{\mathrm{avg}} \approx 9$ K, which are positive, indicating predominately ferromagnetic interactions for $RuBr_3$, as seen before in $RuCl_3$. In Fig. 2d we further analyze how the best-fit Weiss constants evolve for other choices of Δ. Indeed, for a wide range of reasonable Δ around the first-principles value (indicated by the dashed vertical line), the average Weiss constant Θ^{avg} remains positive.

Importantly, for both materials, a standard residual 'background' term has to be included in the fitting, which in our case, depending on the material ($RuBr_3$ or $RuCl_3$) ranges from $\sim -3.5 \times 10^{-4}$ emu/mol to 1.5×10^{-4}. This is of the same order of magnitude as the corresponding term in RuI_3 (~3 to 8×10^{-4} emu/mol)[26,27]. Since in the former cases an intrinsic Pauli origin can be excluded, this observation also casts doubts on a metallic interpretation of this term in RuI_3. Actually, the two available susceptibility measurements on RuI_3 display different behaviors, one nearly temperature-independent[26], and the other[27] showing a Curie-like rise at low temperatures, where a standard CW fit yields $\mu_{\mathrm{eff}} = 0.53\mu_B$ and $\Theta^{\mathrm{avg}}_{\mathrm{CW}} = -3$ K[27]. These differences are consistent with our hypothesis that the measured samples consist of magnetic insulating grains surrounded by metallic boundaries. Then, the samples with larger resistivity data[27] hint at larger insulating grains, hence less metallic boundaries are present, leading to the low-temperature Curie-like upturn in the susceptibility, compared to the samples in ref. [26].

Electronic and magnetic calculations

In the following, we present a comparison of the electronic and magnetic properties of the trihalide RuX_3 family obtained from a combination of density functional theory (DFT) and exact diagonalization of ab-initio-derived low-energy models. Details of the calculations are given in the "Methods" section.

Past experience with first-principles calculations for the Ru-based trihalides[4,7,38–40] indicates that the magnetic order and, to a considerably lesser extent, metallicity is very fragile, with several closely competing different magnetic phases. The ground states may vary depending on small changes in the crystal structure, on the way in which strong correlations are accounted for, and even on tiny details of the computational protocol. With this in mind, it is imperative to compare the calculated properties across the series, using the exact same computational setup.

For the electronic structure calculations, we consider the experimentally reported C2/m[4,9] and $R\bar{3}$[41] structures for $RuCl_3$, and the suggested $R\bar{3}$ structures for $RuBr_3$[25] and RuI_3[27]. Structural details of the four models are summarized in the Supplementary Information. For $RuCl_3$, the $R\bar{3}$ results are shown in Supplementary Information due to very similar results to the C2/m ones.

Figure 3 shows the relativistic density of states (DOS) obtained within GGA + SOC + U as implemented in Wien2k, where a zigzag magnetic configuration with magnetic moments polarized perpendicular to the *ab* plane was considered. For the choice of $U_{\mathrm{eff}} = U - J$ we take as a reference the ab initio estimates for the orbitally-averaged Hubbard on-site (U_{avg}) and Hund's coupling (J_{avg}) as obtained from constrained random-phase approximation (cRPA) calculations (see the "Methods" section for calculation details). In contrast to previous cRPA estimates for $RuCl_3$[42], our estimates incorporate all five *d* orbitals and extend to the complete Ru-based trihalide family. As shown in Fig. 4a, the effective Hubbard interaction parameters decrease with increasing ligand atomic number from Cl to I, which can be attributed to the more delocalized nature of the Ru *d* orbitals in RuI_3 compared to $RuCl_3$ when hybridizing with I instead of Cl.

For $RuCl_3$ a $U_{\mathrm{eff}} = 2.7$ eV yields both the fundamental and direct gap to be ≈1 eV (Fig. 3a) in agreement with the reported optical gap, apart from the presence of multiplets at 200 meV[43]. We systematically reduced U_{eff} to 2.1 eV for $RuBr_3$ and 1.4 eV for RuI_3 following the trend given by the cRPA results. With these values, $RuBr_3$ shows a gap of 0.56 eV (Fig. 3b), while RuI_3 shows a small gap of 0.1 eV (Fig. 3c). The gap closes in RuI_3 when U_{eff} is further reduced to 1 eV. These results indicate a spin–orbit assisted Mott insulating state in disorder-free RuI_3 samples, which is on the verge of a metal–insulator transition. Possibly, as discussed above, a disorder in the experimental samples could act as effective pressure, and bring the samples closer to or over the Mott transition as seen in other Mott insulators[30]. Note that these results hold regardless of the assumed magnetic pattern in the calculations.

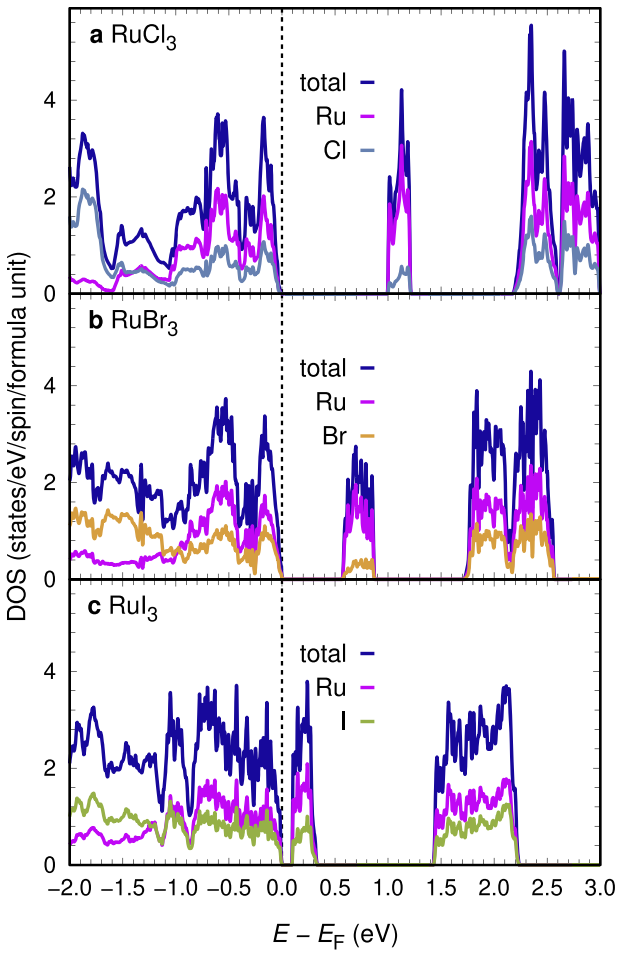

Fig. 3 Density of states for RuX_3 (X = Cl, Br, I). Density of states (DOS) for the experimental structures of $RuCl_3$, $RuBr_3$, and RuI_3, obtained from GGA + SO + U calculations with Wien2k, considering antiferromagnetic zigzag magnetic configurations. For $RuCl_3$ we employed $U_{eff} = 2.7$ eV, for $RuBr_3$ $U_{eff} = 2.1$ eV and for RuI_3 $U_{eff} = 1.4$ eV. Shown is also the contribution of Ru and halogen states to the DOS.

In order to analyze the magnetic structure of the RuX_3 compounds, we first consider spin-polarized total energy calculations with VASP in the GGA + SOC + U approximation (see also the "Methods" section). Detailed results are listed in the Supplementary Information. For $RuCl_3$, the calculated energy of the ferromagnetic state E_{FM} is very competitive with the energy of the experimentally observed zigzag ordered state E_{ZZ}: $E_{ZZ} - E_{FM} \approx 2$ meV/Ru. This observation is consistent with the evidence for a metastable ferromagnetic state in $RuCl_3$[37,44]. Correspondingly, in our effective pseudospin model of $RuCl_3$ discussed below, classically, the energy of the ferromagnet is below that of zigzag, and only by including quantum fluctuations the zigzag ground state is recovered (as in, e.g., ref. [37]). For $RuBr_3$ we find an energy minimum for the zigzag ordering in agreement with the experiment. Interestingly, for RuI_3 Néel and zigzag orders are energetically almost degenerate $E_{Néel} - E_{ZZ} \approx 1$ meV/Ru, with the rest of magnetic orders we scanned being energetically rather close. All orders show very small and varying magnetic moments for Ru. These results hint at a magnetic frustration.

We proceed with the derivation of magnetic exchange models. In the first place, the magnetic Hamiltonian of $RuBr_3$ has been suggested to be closer to the pure Kitaev limit than in $RuCl_3$[25], and, secondly, with our proposed scenario of a Mott insulating state for RuI_3, the question of its magnetic properties is open. To investigate these issues from the first principles, we derive via the ab-initio projED method[45] the pseudospin models $\mathcal{H}_{\text{eff}} = \sum_{ij} \mathbf{S}_i \cdot \mathbb{J}_{ij} \cdot \mathbf{S}_j$ of the three RuX_3 compounds. Here, $\mathbf{S}$ stands for the relativistic pseudospin $j_{\text{eff}} = 1/2$ moment[2].

In the conventional parametrization of Kitaev materials, the exchange matrix $\mathbb{J}_{ij}$ in $R\bar{3}$ symmetry on a nearest-neighbor Z_1-bond (defined in Fig. 1) follows the form

$$\mathbb{J}_{ij} = \begin{pmatrix} J_1 + \nu_1 & \Gamma_1 & \Gamma_1' + \eta_1 \\ \Gamma_1 & J_1 - \nu_1 & \Gamma_1' - \eta_1 \\ \Gamma_1' + \eta_1 & \Gamma_1' - \eta_1 & J_1 + K_1 \end{pmatrix}, \quad (1)$$

with the isotropic Heisenberg exchange J_1, the bond-dependent anisotropic Kitaev exchange K_1, the bond-dependent off-diagonal exchange terms Γ_1 and Γ_1' and correction terms η_1 and ν_1. The latter correction terms are found to be small in our calculated Hamiltonians, and are neglected in what follows. The exchange matrices on X- and Y-bonds follow by respective C_3 rotations about the out-of-plane axis ([111] in pseudospin coordinates). Analogously follow the definitions for second and third neighbor exchange terms (or see, e.g., ref. [8]).

Using U_{avg} and J_{avg} from cRPA (Fig. 4a), the complex hopping parameters extracted from full-relativistic DFT (magnitudes shown in Fig. 4b–d) and the projED method, we extracted the exchange constants shown in Fig. 5b–d.

Evaluating the magnetic interactions of the complete RuX_3 family, we find a nearest-neighbor ferromagnetic Kitaev interaction K_1 to be the dominant in all three compounds. Additionally, a subdominant ferromagnetic nearest-neighbor Heisenberg exchange J_1 is present, which is, however, almost vanishing for the iodine case. The symmetric off-diagonal Γ_1 interaction is of similar magnitude as J_1, changing sign going from Cl and Br to I. Γ_1', often neglected in the $RuCl_3$ analysis, may become rather important, particularly for RuI_3. Further-neighbor interactions are generally smaller than their nearest-neighbor counterparts for all three systems, but increase for larger ligand atomic number and may play, especially in RuI_3, an important role.

That the anisotropic interactions do not monotonically increase with stronger spin-orbit coupling of halogen elements can be related to the SOC source. In the original Jackeli-Khaliullin mechanism[2], the heavy magnetic ions are solely responsible for SOC effects, which can be well described within the SOC atomic limit. In the case of $RuBr_3$ and RuI_3, however, ligand SOC starts to play an important role. To evaluate the interplay of these two SOC sources, we extracted ab initio values for the RuX_3 materials and compared them to the SOC atomic limit (see Supplementary Information). We find that in these compounds SOC effects from magnetic ions and ligands do not enhance each other, but do compete. This leads to the observed inhomogeneous behavior of the magnetic anisotropic terms in Fig. 5 as a function of ligand atomic number. Another consequence of this breakdown of the SOC atomic limit is that the established analytic perturbation theory expressions[2,6,8] become unjustified in Kitaev materials where SOC arises from both the metal and the ligand elements. $RuBr_3$ and RuI_3 are therefore cases where more general approaches, like ours, are indispensable. Another approach would be perturbation theory taking into account ligand orbitals, as recently derived for the $S = 3/2$ material CrI_3[46].

Along the halogen series Cl–Br–I we observe a decrease for nearest-neighbor couplings (Fig. 5b) and an overall increase in magnitude for second and third neighbors (Fig. 5c, d). This can be understood by consideration of the ligand–metal (p–d) hybridization. We quantify the hybridization strength by integrating the DFT(GGA) density of states (DOS) with Ru 4d orbital character in the energy window dominated by the ligand p orbitals (between −7 and −1.05 eV). In spite of respective larger Ru–Ru distances, this can be related to the magnetic exchange by consideration of the ab initio hopping parameters between Wannier d orbitals.

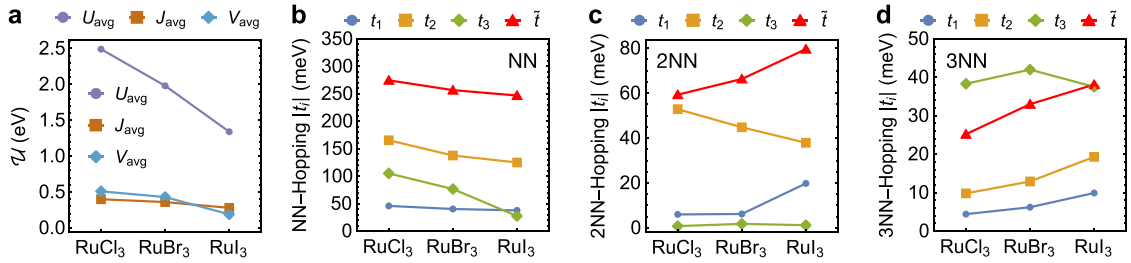

Fig. 4 Ab-initio-computed multi-orbital Hubbard model parameters across the RuX_3 family. a cRPA results for the orbitally averaged on-site Hubbard interaction (U_{avg}), Hund's coupling (J_{avg}), and the nearest-neighbor V_{avg} coupling. **b** Absolute magnitude of hopping parameters $t_1 = t_{(yz,yz)}$, $t_2 = t_{(xz,yz)}$, $t_3 = t_{(xy,xy)}$, and $\tilde{t} = t_{(xy,z^2)}$ on nearest-neighbor (NN), second-neighbor (2NN), and third-neighbor (3NN) Z-bonds.

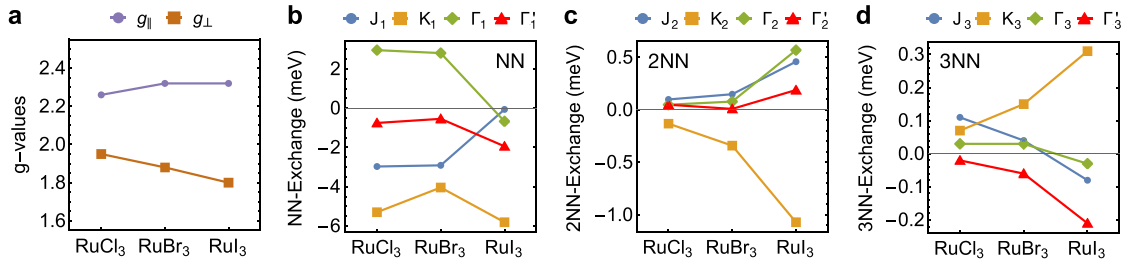

Fig. 5 Ab-initio computed pseudospin models across the RuX_3 family. a Quantum chemistry results for local gyromagnetic g-tensor components $g_\parallel$ (in-plane) and $g_\perp$ (out-of-plane). **b–d** projED results for the magnetic exchange couplings on nearest-neighbor (NN), second-neighbor (2NN), and third-neighbor (3NN) bonds. Tabular form of all values is given in the Supplementary Information.

As also pointed out in ref. [39], in spite of the stronger hybridization the nearest-neighbor hopping parameters are reduced for heavier ligands, illustrated in Fig. 4b. This is reflected in the magnetic exchange parameters (Fig. 5b) in an overall reduced magnitude in the nearest-neighbor parameters. In contrast, the second and third neighbors show a very different dependence on the halogen element. From the dominant further-neighbor hoppings (Fig. 4c, d), the hoppings show an overall tendency to increase, with few exceptions. Certain further-neighbor magnetic exchange parameters, depending on their relation to the individual hopping parameters, become therefore increasingly important for $RuBr_3$ and especially for the magnetic properties of RuI_3.

Finally, we also computed the gyromagnetic g-tensor for the RuX_3 family from first principles, in order to relate the pseudospin $\mathbf{S}$ of the effective Hamiltonian to the magnetic moment $\mathbf{M} = \mu_B \mathbb{G} \cdot \mathbf{S}$. The g-tensor can be approximately characterized by two components, the value parallel to the honeycomb plane, $g_\parallel$, and the one perpendicular to it, $g_\perp$, which are shown in Fig. 5a. We consistently find $g_\parallel > g_\perp$ for the whole family, promoting a stronger Zeeman term for in-plane fields.

We now discuss the ramifications of the derived magnetic models for the magnetism in these materials. For $RuCl_3$, we can compare our result to a vast available literature of models that have been shown to reproduce various experimental observations. Indeed, the model presented here in Fig. 5, derived completely from first principles without adjustments or external parameters, is remarkably close to some well-benchmarked recent models[19,37,38], and is therefore expected to also describe the material quite well. As we apply the same ab-initio setup for the new members of the RuX_3 family, we expect our models to be reliable for them too.

The direction-averaged Weiss constant (Θ_{CW}^{avg} in Table 2) is predicted to be positive across the RuX_3 family, characteristic of ferromagnetic exchange interactions. This is in line with our analysis of the experimental magnetic susceptibilities of $RuCl_3$ and $RuBr_3$ above (Fig. 2). While in $RuCl_3$ and $RuBr_3$ a large FM contribution to the Weiss constant comes from a significant FM nearest-neighbor Heisenberg interaction J_1, this interaction nearly vanishes for RuI_3 (Fig. 5b), leading to a smaller Weiss constant. Furthermore, the small J_1 in RuI_3 renders the nearest-neighbor interactions to be extremely anisotropic, with a dominant Kitaev interaction K_1. While at first glance this might suggest a spin-liquid ground state in RuI_3, the increased strength of the further-neighbor interactions in RuI_3 (see, e.g., J_2, K_2 in Fig. 5c) also needs to be considered[47].

Table 2. Properties of derived pseudospin models.

RuX_3	$RuCl_3$	$RuBr_3$	RuI_3
Θ_{CW}^{avg}	+39.1 K	+35.6 K	+15.4 K
GS	Zigzag	Zigzag	QSL?
$\phi_{\mathbf{M}}$	90°	90°	
$\theta_{\mathbf{M}}$	34.4°	32.4°	

Θ_{CW}^{avg} is the powder-averaged Weiss temperature of each model. 'GS' refers to the ground state computed by exact diagonalization, and the angles of the magnetic moment ϕ_M, θ_M are defined according to Fig. 1b.

To find the magnetic ground state properties, we perform exact diagonalization (ED) calculations of the derived $j_{eff} = 1/2$ models on the 24-site cluster shown in Fig. 6a. In Table 2 and Fig. 6b we summarize the encountered ground states, i.e. zigzag for $RuCl_3$ and $RuBr_3$, and possibly a quantum spin liquid (QSL) in RuI_3. This is discussed in detail below.

For $RuCl_3$, the model in Fig. 5 (as well as the $R\bar{3}$ model discussed in the Supplementary Information) yields zigzag AFM order, identifiable by a maximum at $\mathbf{k} = \mathrm{M}$ in the static spin structure factor, shown in Fig. 6b. The computed ordered magnetic moment direction (see the "Methods" section), parametrized by θ and ϕ in Table 2 (compare Fig. 1b), is found to be tilted by $\theta_{\mathbf{M}} \approx 34°$ out of the plane, in excellent agreement with the recent experiment,

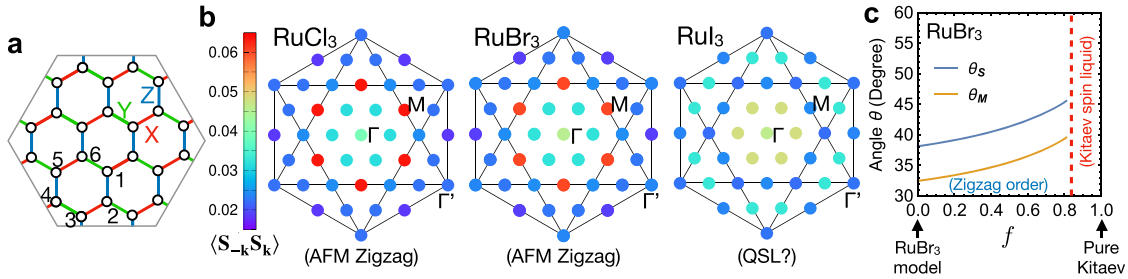

Fig. 6 Exact diagonalization of RuX_3 pseudospin models. a Employed periodic cluster. Labeled sites $1,\ldots,6$ define the Kitaev plaquette operator $W_p = 2^6 S_1^x S_2^y S_3^z S_4^x S_5^y S_6^z$. **b** Static spin structure factor in reciprocal space. Inner (outer) hexagon mark the edge of the first (third) Brillouin Zone. High-symmetry k-points $\Gamma, \mathrm{M}, \Gamma'$ are labeled. Color scale is the same for all three plots. **c** Out-of-plane angle $\theta_{\mathbf{S}}$ ($\theta_{\mathbf{M}}$) of the pseudospin (magnetic moment) within the zigzag phase when tuning from the $RuBr_3$ model ($f=0$) towards the pure Kitaev model ($f=1$). Dashed vertical line indicates phase transition to the Kitaev spin liquid, identified by a peak in $-\partial^2 E/\partial f^2$.

where $\theta_{\mathbf{M}} = 32 \pm 3°$[36] was reported. Interestingly, on the classical level, the ferromagnetic state is lower in energy than the zigzag state, meaning that the latter only becomes the ground state through quantum fluctuations, as discussed also in ref. [37].

We will now focus on the recently synthesized compounds, starting with $RuBr_3$. The static spin structure factor for the $RuBr_3$ model of Fig. 5 is shown in Fig. 6b, indicating also a zigzag AFM order ($\mathbf{k} = \mathrm{M}$ and C_6-rotated vectors), in agreement with experiment[25]. However, the calculated tilt angle of the magnetic moment, $\theta_{\mathbf{M}} = 32°$, is more in line with $RuCl_3$ than with the reported measured $\theta_{\mathbf{M}} = 64°$ of $RuBr_3$[25]. The authors of ref. [25] argued that this anomalously large tilt angle indicates an exceptionally strong relative Kitaev coupling, i.e., larger $|K_1/J_1|$ and $|K_1/\Gamma_1|$ compared to $RuCl_3$. To investigate to what extent closer proximity to the pure Kitaev model could produce such high tilt angles, we take our $RuBr_3$ Hamiltonian of Fig. 5 as a starting point and tune it towards the pure Kitaev model, where K_1 is the only non-zero coupling. This is done by multiplying every exchange coupling except K_1 by $(1-f)$ and sweeping f from 0 to 1. As shown in Fig. 6c, the moment indeed rotates further away from the honeycomb plane upon moving towards the pure Kitaev model, however even right before the transition to the Kitaev spin liquid (indicated by the vertical dashed line), $\theta_{\mathbf{S}}$ does not exceed 46°. $\theta_{\mathbf{M}} = \arccos\left(\frac{\cos\theta_{\mathbf{S}}}{\sqrt{g_\parallel{}^2\cos^2\theta_{\mathbf{S}} + g_\perp{}^2\sin^2\theta_{\mathbf{S}}}}\right)$, which is to be compared to the neutron diffraction experiment, is even smaller due to the anisotropy $g_\parallel > g_\perp$ in our calculated g-tensor (Fig. 5a). A reconciliation with the reported $\theta_{\mathbf{M}} = 64°$ would therefore require quite drastic changes to the g-tensor anisotropy and/or the exchange parameters. While in the whole J_1–K_1–Γ_1 parameter space with $\Gamma_1 > 0$, no angles of $\theta_{\mathbf{S}}$ beyond ~ 40° are expected in the zigzag phase[48], significant *negative* $\Gamma_1 < 0$ can in principle lead to $\theta_{\mathbf{S}}$ beyond 60°[49]. However such terms seem incompatible with the ab-initio results and would likely need strong distortions from the present considered $RuBr_3$ crystal structure to be realized.

More distinct from the other two compounds are our results for RuI_3. As discussed above, in our GGA + SOC + U calculations we find a very flat energy landscape of competitive magnetic configurations, indicative of strong magnetic frustration. Fittingly, the ground state from the exact diagonalization of the present exchange model does not show a dominant ordering wave vector in the spin structure factor (see Fig. 6b). Although this is a signature generally associated with quantum spin liquid (QSL) states, we note that in the present model, the Kitaev $\mathbb{Z}_2$ flux operator yields $\langle W_\mathrm{p}\rangle = 2^6\langle S_1^x S_2^y S_3^z S_4^x S_5^y S_6^z\rangle \approx 0.29$ (site indices refer to Fig. 6a). While this is clearly elevated compared to classical collinear states, where $\langle W_p\rangle$ is restricted to $|\langle W_\mathrm{p}\rangle| \leq \frac{1}{27} < 0.04$, it is still significantly below the value of the pure unperturbed Kitaev spin liquid, where $\langle W_\mathrm{p}\rangle = 1$[1]. Hence, if the ground state constitutes a QSL state, it is presumably not the $\mathbb{Z}_2$ Kitaev spin liquid. The precise nature of the encountered magnetically disordered state might be interesting for future studies. It appears to be stabilized by the further-neighbor interactions, as we find a clear ferromagnetic ground state when omitting the second- and third-neighbor interactions in the present model. While a QSL scenario for our full RuI_3 model is compelling, we note that finite-size effects in our calculation could play a role. In particular, the finite-size cluster could be incompatible with the supposed correct ordering wave vector of the model, e.g. in the case of an incommensurate ordering vector.

To summarize, we have presented a comparative analysis of the electronic and magnetic properties of the Ru-based trihalide family, including the recently synthesized $RuBr_3$ and RuI_3, by combining state-of-the-art ab initio microscopic modeling with analysis of reported resistivity, specific heat, and magnetic susceptibility data. The evolution of the magnetic order and Mott–Hubbard correlations along the halogen series, as well as the possible role of disorder, have been a central part of our study. We conclude that:

1. All three ideal compounds are spin–orbit-assisted Mott insulators, but their fundamental gap decreases with higher ligand atomic number, Cl → Br → I, with RuI_3 coming rather close to a metal–insulator transition.
2. From DFT total-energy calculations, in ideal, pristine crystals the zigzag magnetic order is even more stable in $RuBr_3$ than in $RuCl_3$, while RuI_3 shows significant magnetic frustration. Our ab-initio extracted low-energy models predict RuI_3 to feature either an incommensurate magnetic ordered state or a quantum spin liquid, which, interestingly, is possibly of a different kind to the $\mathbb{Z}_2$ Kitaev spin liquid.
3. A number of reported experimental observations seem to be adversely affected by the sample quality, in particular by dirty grain boundaries. In fact, most of the observations in RuI_3 can be reconciled with theory by assuming insulating grains surrounded by (bad) metallic boundaries. The experimental evidence is consistent with a 'dirty' insulator, or a bad metal. Disorder would favor either of these.
4. In all three systems the dominant nearest-neighbor interaction is FM Kitaev K_1, with a subdominant FM Heisenberg Interaction J_1, that nearly vanishes for RuI_3. We observe a non-monotonous behavior of the magnetic anisotropic terms as a function of ligand atomic number that we trace back to a competition of the SOC effects from magnetic ions and ligands.
5. $RuBr_3$ has predominantly ferromagnetic interactions, in contrast to what is suggested by standard Curie–Weiss analysis[25]. Such interactions are consistent with the experimental susceptibility when taking into account high-temperature SOC effects. Our ab-initio magnetic model predicts zigzag order in agreement with the

experiment, with a tilting angle of $\theta_{\mathbf{M}} = 32°$ for the magnetic moments, similar to $RuCl_3$, but in contradiction to the reported $\theta_{\mathbf{M}} = 64°$[25]. We showed that such a large angle cannot be simply explained by proximity to the pure Kitaev model, but would require quite drastic changes to the exchange parameters, such as sizeable negative $\Gamma_1 < 0$. Those would necessitate strong distortions on the reported $RuBr_3$ crystal structures.

Answering the question posed in the title, our results and analysis strongly suggest that the ideal $RuCl_3$, $RuBr_3$, and RuI_3 compounds constitute a family of three Mott-insulating *siblings*. The challenging task of getting better samples will hopefully help resolve the open issues.

METHODS

Modified Curie–Weiss fit of $RuBr_3$

We fit the experimental average susceptibility of ref. [25] with four fitting parameters $\chi_0^{\perp}, \chi_0^{\parallel}, \Theta^{\perp}, \Theta^{\parallel}$ using the modified Curie–Weiss formula

$$\chi^{\mathrm{avg}}(T) \approx \frac{2}{3}\left(\chi_0^{\parallel} + \frac{C^{\parallel}(T)}{T-\Theta^{\parallel}}\right) + \frac{1}{3}\left(\chi_0^{\perp} + \frac{C^{\perp}(T)}{T-\Theta^{\perp}}\right), \tag{2}$$

where $\Theta^{\parallel}$, $\Theta^{\perp}$ are the Weiss constants and $C^{a}(T) \propto [\mu^{a}_{\mathrm{eff}}(T,\Delta)]^2$ is determined through Δ as described in ref. [33]. Superscripts $\parallel$ and $\perp$ indicate the in- and out-of-honeycomb-plane direction, respectively. The susceptibility is fitted over the temperature range 150–300 K and SOC strength $\lambda = 0.15$ eV is taken.

DFT calculations

To make sure that the calculated features within density functional theory are robust with respect to the choice of the basis set, we have tested the results using two different methods: the projector augmented wave method[50,51] as implemented in the VASP code[52,53], and the full potential linearized augmented plane-wave (LAPW) basis as implemented in Wien2k[54]. Throughout the paper, we have used the generalized gradient approximation (GGA[55]) for the exchange-correlation functional. Hubbard correlation effects were included on a mean-field level in the rotationally invariant implementation of the GGA + U method[56]. All calculations included spin–orbit coupling (SOC) effects. For VASP we used the Ru_pv pseudopotential, treating Ru *p* states as valence, and the standard pseudopotentials for the halogens. The Γ-centered $8\times8\times8$ mesh in the nonmagnetic rhombohedral Brillouin zone was used, or the correspondingly scaled meshes for other structures. The energy cut-off was 350 eV, and the energy convergence criterion 1×10^{-08} eV. For each type of magnetic order, a number of collinear starting configurations with randomly selected Néel vectors were used, and the lowest-energy result was selected as the ground state. Individual results can be found in the Supplementary Information. For Wien2k we chose the plane-wave cutoff $K_{\max}$ corresponding to $RK_{\max} = 8$ and a $\mathbf{k}$ mesh of $8\times8\times2$ for the $R\bar{3}$ structure in the hexagonal Brillouin zone and $8\times4\times6$ in the first Brillouin zone of the conventional unit cell for the *C*/2*m* structure. The density of states are calculated using a $\mathbf{k}$ mesh of $12\times12\times3$ for the $R\bar{3}$ structure and $12\times6\times9$ for the *C*/2*m* structure. The zigzag configurations are constructed using a conventional cell of the *C*/2*m* structure for $RuCl_3$ while a $1\times2\times1$ supercell of the $R\bar{3}$ structures for $RuBr_3$ and $RuCl_3$.

cRPA calculations

In order to obtain ab-initio estimates for the effective Coulomb interaction for the Ru-trihalide family, we employed the constrained random-phase approximation (cRPA)[57,58], as implemented in the FHI-gap code[59], based on the Wien2K electronic structure. The low-energy limit of the screened interaction was projected on the five Ru *d* orbitals, where screening processes in the same window were excluded. Convergence with respect to the discretization of the Brillouin zone and energy cutoff was ensured.

DFT-based derivation of magnetic models

To derive bilinear exchange parameters for each material, we employed the projED method[45], which consists of two steps. First, complex ab-initio hopping parameters between the ruthenium ions are estimated with projective Wannier functions[60] applied on full relativistic FPLO[61] calculations on a $12\times12\times12\mathbf{k}$ mesh. This allows constructing an effective electronic model $\mathcal{H}_{\mathrm{tot}} = \mathcal{H}_{\mathrm{hop}} + \mathcal{H}_{\mathrm{U}}$, where the complex ab-initio hopping parameters enter the kinetic term $\mathcal{H}_{\mathrm{hop}} = \sum_{ij\alpha\beta}\sum_{\sigma\sigma'} t_{i\alpha,j\beta}^{\sigma\sigma'} c_{i\alpha\sigma}^{\dagger} c_{j\beta\sigma'}$ and the cRPA effective Coulomb interaction parameters enter the two-particle term $\mathcal{H}_{\mathrm{U}} = \sum_{i\alpha\beta\gamma\delta}\sum_{\sigma\sigma'} U_{i\alpha\beta\gamma\delta}^{\sigma\sigma'} c_{i\alpha\sigma}^{\dagger} c_{i\beta\sigma'}^{\dagger} c_{i\delta\sigma'} c_{i\gamma\sigma}$. Second, the effective spin Hamiltonian $\mathcal{H}_{\mathrm{eff}}$ is extracted from the electronic model via exact diagonalization (ED) and projection of the resulting energy spectrum onto the low-energy subspace, mapped onto pseudo-spin operator representation in the j_{eff} picture with the projection operator $\mathbb{P}$: $\mathcal{H}_{\mathrm{eff}} = \mathbb{P}\mathcal{H}_{\mathrm{tot}}\mathbb{P} = \sum_{ij} \mathbf{S}_i \mathbb{J}_{ij} \mathbf{S}_j$.

Note that for $RuCl_3$ the exchange constants slightly differ from previously calculated values by some of the authors[8,38]. The reason for this lies in the following details of the calculation setup: (i) first principles input parameters U_{avg} and J_{avg} from cRPA in contrast to previous choices, (ii) consideration of all five 4*d* ruthenium orbitals with the cost of restriction onto two-site clusters, (iii) SOC effects from both Ru^{3+} and ligands considered through complex hopping parameters in contrast to the atomic limit, and (iv) consideration of the experimental crystal structure in contrast to relaxed ambient pressure structure as it was done in ref. [38].

For the calculation of the gyromagnetic *g*-tensor, we considered $[RuX_6]^{3-}$ molecules within the quantum chemistry ORCA 3.03 package[62,63] with the functional TPSSh, basis set def2-TZVP and complete active space for the *d* orbitals CAS(5,5).

Exact diagonalization

Exact diagonalization calculations of the $j_{\mathrm{eff}} = 1/2$ models were performed on the 24-site cluster shown in Fig. 6a. To identify possible magnetic ordering, we analyze the static spin structure factor $\sum_{\mu=x,y,z}\langle S^{\mu}_{-\mathbf{k}} S^{\mu}_{\mathbf{k}}\rangle$. For the ordered moment direction, we compute the eigenvector with the maximal eigenvalue of the correlation matrix $(\langle S^{\mu}_{-\mathbf{k}} S^{\nu}_{\mathbf{k}}\rangle)_{\mu,\nu}$ $(\mu,\nu\in\{x,y,z\})$ at the ordering wave vector $\mathbf{k} = \mathbf{Q}$. This eigenvector then represents the ordered *pseudospin* direction $\mathbf{S}$[49], which relates to the magnetic moment direction $\mathbf{M} \propto \mathbb{G}\cdot\mathbf{S}$, as measured by neutron diffraction, via the anisotropic *g*-tensor $\mathbb{G}$.

DATA AVAILABILITY

The datasets generated during the current study are available from the corresponding authors upon reasonable request.

CODE AVAILABILITY

The custom codes implementing the calculations of this study are available from the authors upon reasonable request.

Received: 21 March 2022; Accepted: 6 July 2022;
Published online: 29 July 2022

REFERENCES

1. Kitaev, A. Anyons in an exactly solved model and beyond. *Ann. Phys.* **321**, 2–111 (2006).
2. Jackeli, G. & Khaliullin, G. Mott insulators in the strong spin–orbit coupling limit: from Heisenberg to a quantum compass and Kitaev models. *Phys. Rev. Lett.* **102**, 017205 (2009).
3. Plumb, K. W. et al. α-$RuCl_3$: a spin-orbit assisted Mott insulator on a honeycomb lattice. *Phys. Rev. B* **90**, 041112 (2014).
4. Johnson, R. D. et al. Monoclinic crystal structure of α-$RuCl_3$ and the zigzag antiferromagnetic ground state. *Phys. Rev. B* **92**, 235119 (2015).
5. Zhou, X. et al. Angle-resolved photoemission study of the Kitaev candidate α-$RuCl_3$. *Phys. Rev. B* **94**, 161106 (2016).
6. Rau, J. G., Lee, E. K.-H. & Kee, H.-Y. Generic spin model for the honeycomb iridates beyond the Kitaev limit. *Phys. Rev. Lett.* **112**, 077204 (2014).
7. Kim, H.-S. & Kee, H.-Y. Crystal structure and magnetism in α-$RuCl_3$: an ab initio study. *Phys. Rev. B* **93**, 155143 (2016).
8. Winter, S. M., Li, Y., Jeschke, H. O. & Valentí, R. Challenges in design of Kitaev materials: magnetic interactions from competing energy scales. *Phys. Rev. B* **93**, 214431 (2016).
9. Cao, H. B. et al. Low-temperature crystal and magnetic structure of α-$RuCl_3$. *Phys. Rev. B* **93**, 134423 (2016).

10. Banerjee, A. et al. Neutron scattering in the proximate quantum spin liquid α-$RuCl_3$. *Science* **356**, 1055–1059 (2017).
11. Sandilands, L. J., Tian, Y., Plumb, K. W., Kim, Y.-J. & Burch, K. S. Scattering continuum and possible fractionalized excitations in α-$RuCl_3$. *Phys. Rev. Lett.* **114**, 147201 (2015).
12. Nasu, J., Knolle, J., Kovrizhin, D. L., Motome, Y. & Moessner, R. Fermionic response from fractionalization in an insulating two-dimensional magnet. *Nat. Phys.* **12**, 912–915 (2016).
13. Do, S.-H. et al. Majorana fermions in the Kitaev quantum spin system α-$RuCl_3$. *Nat. Phys.* **13**, 1079–1084 (2017).
14. Widmann, S. et al. Thermodynamic evidence of fractionalized excitations in α-$RuCl_3$. *Phys. Rev. B* **99**, 094415 (2019).
15. Sears, J. A., Zhao, Y., Xu, Z., Lynn, J. W. & Kim, Y.-J. Phase diagram of α-$RuCl_3$ in an in-plane magnetic field. *Phys. Rev. B* **95**, 180411 (2017).
16. Banerjee, A. et al. Excitations in the field-induced quantum spin liquid state of α-$RuCl_3$. *npj Quantum Mater.* **3**, 8 (2018).
17. Kasahara, Y. et al. Majorana quantization and half-integer thermal quantum Hall effect in a Kitaev spin liquid. *Nature* **559**, 227 (2018).
18. Hentrich, R. et al. Unusual phonon heat transport in α-$RuCl_3$: strong spin–phonon scattering and field-induced spin gap. *Phys. Rev. Lett.* **120**, 117204 (2018).
19. Winter, S. M. et al. Breakdown of magnons in a strongly spin-orbital coupled magnet. *Nat. Commun.* **8**, 1152 (2017).
20. Hentrich, R. et al. High-field thermal transport properties of the Kitaev quantum magnet α-$RuCl_3$: evidence for low-energy excitations beyond the critical field. *Phys. Rev. B* **102**, 235155 (2020).
21. Sahasrabudhe, A. et al. High-field quantum disordered state in α-$RuCl_3$: spin flips, bound states, and multiparticle continuum. *Phys. Rev. B* **101**, 140410 (2020).
22. Chern, L. E., Zhang, E. Z. & Kim, Y. B. Sign structure of thermal hall conductivity and topological magnons for in-plane field polarized Kitaev magnets. *Phys. Rev. Lett.* **126**, 147201 (2021).
23. Czajka, P. et al. Oscillations of the thermal conductivity in the spin-liquid state of α-$RuCl_3$. *Nat. Phys.* **17**, 915–919 (2021).
24. Lefrançois, É. et al. Evidence of a phonon Hall effect in the Kitaev spin liquid candidate α-$RuCl_3$. *Phys. Rev. X* **12**, 021025 (2022).
25. Imai, Y. et al. Zigzag magnetic order in the Kitaev spin-liquid candidate material $RuBr_3$ with a honeycomb lattice. *Phys. Rev. B* **105**, L041112 (2022).
26. Nawa, K. et al. Strongly electron-correlated semimetal RuI_3 with a layered honeycomb structure. *J. Phys. Soc. Jpn.* **90**, 123703 (2021).
27. Ni, D., Gui, X., Powderly, K. M. & Cava, R. J. Honeycomb-structure RuI_3, a new quantum material related to α-$RuCl_3$. *Adv. Mater.* **34**, 2106831 (2022).
28. Jaramillo, R., Ha, S. D., Silevitch, D. M. & Ramanathan, S. Origins of bad-metal conductivity and the insulator–metal transition in the rare-earth nickelates. *Nat. Phys.* **10**, 304–307 (2014).
29. Little, A. et al. Antiferromagnetic resonance and terahertz continuum in α-$RuCl_3$. *Phys. Rev. Lett.* **119**, 227201 (2017).
30. Gati, E. et al. Effects of disorder on the pressure-induced Mott transition in κ-$(BEDT\text{-}TTF)_2Cu[N(CN)_2]Cl$. *Crystals* **8**, 38 (2018).
31. Tanaka, O. et al. Thermodynamic evidence for a field-angle-dependent Majorana gap in a Kitaev spin liquid. *Nat. Phys.* **18**, 429–435 (2022).
32. Sears, J. A. et al. Magnetic order in α-$RuCl_3$: a honeycomb-lattice quantum magnet with strong spin–orbit coupling. *Phys. Rev. B* **91**, 144420 (2015).
33. Li, Y., Winter, S. M., Kaib, D. A. S., Riedl, K. & Valentí, R. Modified Curie–Weiss law for j_{eff} magnets. *Phys. Rev. B* **103**, L220408 (2021).
34. Winter, S. M. et al. Models and materials for generalized Kitaev magnetism. *J. Condens. Matter Phys.* **29**, 493002 (2017).
35. Laurell, P. & Okamoto, S. Dynamical and thermal magnetic properties of the Kitaev spin liquid candidate α-$RuCl_3$. *npj Quantum Mater.* **5**, 2 (2020).
36. Sears, J. A. et al. Ferromagnetic Kitaev interaction and the origin of large magnetic anisotropy in α-$RuCl_3$. *Nat. Phys.* **16**, 837–840 (2020).
37. Suzuki, H. et al. Proximate ferromagnetic state in the Kitaev model material α-$RuCl_3$. *Nat. Commun.* **12**, 4512 (2021).
38. Kaib, D. A. S., Biswas, S., Riedl, K., Winter, S. M. & Valentí, R. Magnetoelastic coupling and effects of uniaxial strain in α-$RuCl_3$ from first principles. *Phys. Rev. B* **103**, L140402 (2021).
39. Kim, H.-S. Spin-orbit-entangled nature of magnetic moments and Kitaev magnetism in layered halides. *Appl. Sci. Converg. Technol.* **30**, 191–194 (2021).
40. Zhang, Y., Lin, L.-F., Moreo, A. & Dagotto, E. Theoretical study of the crystal and electronic properties of α-RuI_3. *Phys. Rev. B* **105**, 085107 (2022).
41. Park, S.-Y. et al. Emergence of the isotropic Kitaev honeycomb lattice with two-dimensional Ising universality in α-$RuCl_3$. Preprint at https://arxiv.org/abs/1609.05690 (2016).
42. Eichstaedt, C. et al. Deriving models for the Kitaev spin-liquid candidate material α-$RuCl_3$ from first principles. *Phys. Rev. B* **100**, 075110 (2019).
43. Sandilands, L. J. et al. Spin–orbit excitations and electronic structure of the putative Kitaev magnet α-$RuCl_3$. *Phys. Rev. B* **93**, 075144 (2016).
44. Bachus, S. et al. Thermodynamic perspective on field-induced behavior of α-$RuCl_3$. *Phys. Rev. Lett.* **125**, 097203 (2020).
45. Riedl, K., Li, Y., Valentí, R. & Winter, S. M. Ab initio approaches for low-energy spin Hamiltonians. *Phys. Status Solidi B* **256**, 1800684 (2019).
46. Stavropoulos, P. P., Liu, X. & Kee, H.-Y. Magnetic anisotropy in spin-3/2 with heavy ligand in honeycomb Mott insulators: application to CrI_3. *Phys. Rev. Res.* **3**, 013216 (2021).
47. Rousochatzakis, I., Reuther, J., Thomale, R., Rachel, S. & Perkins, N. B. Phase diagram and quantum order by disorder in the Kitaev K_1-K_2 honeycomb magnet. *Phys. Rev. X* **5**, 041035 (2015).
48. Rusnačko, J., Gotfryd, D. & Chaloupka, J. Kitaev-like honeycomb magnets: global phase behavior and emergent effective models. *Phys. Rev. B* **99**, 064425 (2019).
49. Chaloupka, J. & Khaliullin, G. Magnetic anisotropy in the Kitaev model systems Na_2IrO_3 and $RuCl_3$. *Phys. Rev. B* **94**, 064435 (2016).
50. Blöchl, P. E. Projector augmented-wave method. *Phys. Rev. B* **50**, 17953–17979 (1994).
51. Kresse, G. & Joubert, D. From ultrasoft pseudopotentials to the projector augmented-wave method. *Phys. Rev. B* **59**, 1758–1775 (1999).
52. Kresse, G. & Hafner, J. Ab initio molecular dynamics for liquid metals. *Phys. Rev. B* **47**, 558–561 (1993).
53. Kresse, G. & Furthmüller, J. Efficiency of ab-initio total energy calculations for metals and semiconductors using a plane-wave basis set. *Comput. Mater. Sci.* **6**, 15–50 (1996).
54. Blaha, P., Schwarz, K., Madsen, G. K. H., Kvasnicka, D. & Luitz, J. *WIEN2k, an Augmented Plane Wave Plus Local Orbitals Program for Calculating Crystal Properties* (Technische Universität Wien, Austria, 2001).
55. Perdew, J. P., Burke, K. & Ernzerhof, M. Generalized gradient approximation made simple. *Phys. Rev. Lett.* **77**, 3865–3868 (1996).
56. Anisimov, V. I., Solovyev, I. V., Korotin, M. A., Czyżyk, M. T. & Sawatzky, G. A. Density-functional theory and NiO photoemission spectra. *Phys. Rev. B* **48**, 16929–16934 (1993).
57. Aryasetiawan, F. et al. Frequency-dependent local interactions and low-energy effective models from electronic structure calculations. *Phys. Rev. B* **70**, 195104 (2004).
58. Aryasetiawan, F., Karlsson, K., Jepsen, O. & Schönberger, U. Calculations of Hubbard *U* from first-principles. *Phys. Rev. B* **74**, 125106 (2006).
59. Jiang, H. et al. FHI-gap: a GW code based on the all-electron augmented plane wave method. *Comput. Phys. Commun.* **184**, 348–366 (2012).
60. Eschrig, H. & Koepernik, K. Tight-binding models for the iron-based superconductors. *Phys. Rev. B* **80**, 104503 (2009).
61. Koepernik, K. & Eschrig, H. Full-potential nonorthogonal local–orbital minimum-basis band-structure scheme. *Phys. Rev. B* **59**, 1743–1757 (1999).
62. Neese, F. The ORCA program system. *Wiley Interdiscip. Rev. Comput. Mol. Sci.* **2**, 73–78 (2012).
63. Neese, F. Efficient and accurate approximations to the molecular spin–orbit coupling operator and their use in molecular *g*-tensor calculations. *J. Chem. Phys.* **122**, 034107 (2005).

ACKNOWLEDGEMENTS

We thank Stephen M. Winter, Robert J. Cava, Yoshinori Imai, and Elena Gati for discussions and Yoshinori Imai for sharing the structural information of $RuBr_3$ with us before publication. R.V., A.R., K.R. and D.A.S.K. acknowlegde support by the Deutsche Forschungsgemeinschaft (DFG, German Research Foundation) for funding through Project No. 411289067 (VA117/15-1) and TRR 288—422213477 (project A05). Y.L. acknowledges support from the National Natural Science Foundation of China (Grant No. 12004296) and the China Postdoctoral Science Foundation (Grant No. 2019M660249). I.I.M. acknowledges support from the U.S. Department of Energy through grant #DE-SC0021089. R.V. and I.I.M. thank the Wilhelm und Else Heraeus Stiftung for financial support.

AUTHOR CONTRIBUTIONS

R.V. conceived and supervised the project. Density functional theory calculations were performed by K.R., A.R., Y.L., I.I.M., cRPA calculations by S.B., projED calculations by K.R., and calculations on magnetic models by D.A.S.K. All authors contributed to the manuscript.

FUNDING

Open Access funding enabled and organized by Projekt DEAL.

COMPETING INTERESTS

The authors declare no competing interests.

ADDITIONAL INFORMATION

Supplementary information The online version contains supplementary material available at https://doi.org/10.1038/s41535-022-00481-3.

Correspondence and requests for materials should be addressed to David A. S. Kaib, Kira Riedl or Roser Valentí.